GDF15 negatively regulates RGS16 involving in abnormal lipid metabolism in IVF-ET male mice offspring

Jingliu Liu
Institute for Fetology, the First Affiliated Hospital of Soochow University
Yichen Zhu
Jiangsu Key Laboratory of Neuropsychiatric Diseases and Cambridge-Suda Genomic Resource Center
Dan Zhu
Institute for Fetology, the First Affiliated Hospital of Soochow University
Yajun Shi
Institute for Fetology, the First Affiliated Hospital of Soochow University
Likui Lu
Institute for Fetology, the First Affiliated Hospital of Soochow University
Weisheng Li
Institute for Fetology, the First Affiliated Hospital of Soochow University
Lingjun Li
Institute for Fetology, the First Affiliated Hospital of Soochow University
Xiuwen Zhou
Institute for Fetology, the First Affiliated Hospital of Soochow University
Hao Yang
Institute for Fetology, the First Affiliated Hospital of Soochow University
Bin Wang
Institute for Fetology, the First Affiliated Hospital of Soochow University
Miao Sun (miaosunsuda@163.com)
Institute for Fetology, the First Affiliated Hospital of Soochow University

Research Article

Keywords: In vitro fertilization-embryo transfer, Liver, Lipid deposition, GDF15, RGS16

Posted Date: April 27th, 2022

DOI: https://doi.org/10.21203/rs.3.rs-1565536/v1

Abstract

Background

In vitro fertilization and embryo transfer (IVF-ET) is now widely used as a routine assisted reproductive technology (ART) procedure, and the long-term health outcomes of IVF-ET offspring are of great concern. A growing body of research suggests that children conceived through IVF-ET may be at increased risk for metabolic syndrome, type 2 diabetes, and cardiovascular disease.

Methods

An IVF-ET mouse model was established. Body weights and the principal organs were weighed, and organ/body weight indexes were calculated. The glucose metabolism levels were assessed by glucose tolerance test (GTT), insulin tolerance test (ITT), and pyruvate tolerance test (PTT). The quantitative real-time PCR (RT-qPCR) technique was performed to determine the gene expression profiling in livers; HepG2 cells were transfected with either interfering RNA or overexpression plasmids to investigate the gene functions. mRNA and protein expression of relevant genes was verified by RT-qPCR and protein immunoblotting.

Results

Compared with the natural mating control group, male IVF-ET offspring showed: Higher body, liver, and epididymal white adipose tissue (eWAT) weight; Disrupted glucolipid metabolism with abnormal GTT, ITT, and PTT; Significantly decreased GDF15 expression along with increased expression of RGS16. Furthermore, phosphorylation of ERK1/2 and AKT were significantly reduced in the IVF-ET group. *In vitro* HepG2 cell experiment showed that knockdown of GDF15 caused an abnormal increase in RGS16 expression and decreased phosphorylation of ERK1/2 and AKT, accompanied by increased lipid deposition; In contrast, overexpression of GDF15 reduced expression of RGS16. Simultaneous knockdown of both GDF15 and RGS16 reversed lipid deposition in HepG2 cells.

Conclusion

Down-regulation of GDF15 expression in liver tissues of IVF-ET male offspring results in elevated expression of RGS16, which causes the weakening of the downstream ERK1/2 and AKT phosphorylation pathways, leading to increased activity lipid deposition and abnormal lipid metabolism in the liver of IVF-ET male offspring. It is suggested that GDF15-RGS16-p-ERK1/2/p-AKT pathway plays a crucial role in liver lipid deposition in IVF-ET male offspring and could be a potential therapeutic target.

1. Background

Assisted reproductive technology (ART) refers to medical aids that enable infertile couples to conceive. It includes artificial insemination (AI), *in vitro* fertilization and embryo transfer (IVF-ET) and their derivatives [1]. In recent years, the incidences of infertility keep growing, and approximately 17% of couples suffer from infertility conditions worldwide [2]. In China, about 200 thousand IVF babies are born each year. Especially with the unveiled "three-child" policies, in order to resolve fertility problems, the demands for ART have increased dramatically. Consequently, the proportion of children born after IVF keeps rising.

Theories of “gamete and embryo-fetal origins of adult diseases” suggest that adverse environmental exposures during gametogenesis, embryo implantation, and critical developmental stages from fetus to the infant will have an “imprint” impact on the growth and development of offspring, leading to an increased risk of chronic diseases such as hypertension, insulin resistance, type 2 diabetes and centripetal obesity in adulthood [3]. As one of the environmental exposures at early developmental stages, ARTs involve ovarian stimulation, *in vitro* fertilization or intracytoplasmic single sperm injection, embryo culture, freezing, and transfer, all of which mean that the environment experienced by gametes and embryos is significantly altered compared to natural pregnancy [4, 5].

Whether ARTs affect children’s health in the long term has been a topic of great interest since the birth of the first i*n vitro* fertilization (IVF) child in 1978 [6]. A long-term follow-up study shows IVF-ET-born children may be at increased risk of metabolic and cardiovascular disease [7]. It has been reported to increase fasting blood glucose levels [8], blood pressure [8, 9], adiposity, triglyceride levels [10], and vascular dysfunction [9, 11, 12] in IVF children. In our recent studies, we found that umbilical veins of IVF-ET offspring showed abnormal sensitivity to acetylcholine (ACh) or angiotensin II (AII)-mediated contraction, which could be caused by hypo/hypermethylation of the specific receptors [13, 14]. Our findings strongly supported the idea that IVF-ET could directly lead to changes in fetal vessel functions, which might result in cardiovascular disorders in the long term.

However, various causes of infertility and complicated genetic backgrounds in humans make the studies exploring the influence of ART itself on offspring health become too tricky. To eliminate these complicating factors, animal models have been gradually used for studying the potential effects of IVF-ET on its offspring. Recent studies using the IVF-ET mouse model found impaired metabolism in IVF-ET offspring, such as altered fasting blood glucose levels, impaired glucose tolerance and pyruvate [15–19]; increased body weight, body fat, and higher triglyceride, cholesterol, and insulin levels [20]; reduced lipolysis and increased lipid accumulation in adipose tissue and liver tissue [19, 21]. These studies suggest that the IVF-ET technique itself is significantly associated with abnormal metabolic function in the offspring.

Most studies on the effects of assisted reproductive technologies on offspring metabolism have focused on glucose metabolism, while the specific mechanisms of altered lipid metabolism in IVF-ET offspring are seldom studied. Therefore, we generated a C57BL/6N mouse model by IVF-ET technology to learn the liver function and lipid metabolism of IVF-ET offspring and then explored the correlation between IVF-ET technology and the alteration of metabolic function of offspring and the specific mechanism.

2. Materials And Methods

2.1. Animals

All experimental procedures with mice were approved by the Jiangsu Model Organisms Center's Ethical Committee. C57BL/6N mice and ICR mice were purchased from the Beijing Vital River Laboratory Animal Technology and housed in a 12-h alternating light-dark, temperature-controlled, specific pathogen-free barrier facility prior to and throughout experimentation. Pregnant mice were housed in a single cage, and pups were sorted into separate cages four weeks after birth. Mice that need to be measured for food intake are housed in a single cage.

C57BL/6N females and males were used to create 2-cell embryos transferred into the oviducts of pseudopregnancy ICR mice, referred to as the IVF-ET group. In addition, we created a naturally pregnant group as a control group (CON). On the day of birth, the pups were weighed. Weighing continued after weaning (4–28 weeks). Daily food weighing was performed with both groups.

2.2. *In vitro* fertilization

Superovulation in 6-10-week-old female C57BL/6N mice by intraperitoneal injection of 5IU of pregnant horse serum gonadotropin (PMSG, Ningbo Second Hormone Factory, Ningbo, China) followed by 5IU of human chorionic gonadotropin (HCG, Ningbo Second Hormone Factory, Ningbo, China) 48 h. Oocytes were collected from the oviductal pots 13–15 h after HCG administration and fertilized *in vitro* with caudal epididymal sperm from 6-10-week-old male C57BL/6N mice. Gametes were co-cultured in human oviductal fluid medium (HTF, Sigma, USA) in a 5% CO_2 and 5% O_2 incubator (Heal Force, Shanghai, China) at 37°C for 15–16 h. After co-culture, 2-cell embryos were washed with Potassium simplex optimized medium (KSOM, Sigma, USA) three times, followed by embryo transfer.

2.3. Embryo transfer

The 6-8-week-old female ICR mice are used as pseudopregnant recipients for embryo transfer. Recipients were produced by mating with vasectomized male ICR mice. The day on which a plug was observed was considered embryonic day 0.5 (E0.5) of pseudopregnancy. Fresh 2-cell embryos were surgically transferred to the fallopian tubes of pseudopregnant ICR females at E0.5. Mice were anesthetized with tribromoethanol. All-female mice that received embryos were fed standard chow.

2.4. Glucose, Insulin, and Pyruvate tolerance test

Glucose tolerance test (GTT) and pyruvate tolerance test (PTT) were performed at 8 am after 14–16 hours of fasting, and insulin tolerance test (ITT) was performed at 1 pm after 2 hours of fasting. Glucose (2g/kg), pyruvate (2g/kg), or insulin (1IU/kg) were administered intraperitoneally to the mice. Glucose levels were measured using a glucometer (Johnson, America) at 0, 15, 30, 60, 90, and 120 min after injection. GTT, ITT, and PTT were performed at 20–24 weeks of age.

2.5. Lipid parameters

After 4 hours of fasting, blood samples were collected from the posterior orbits of anesthetized mice to extract serum and stored at -80°C. Liver lipids were extracted from approximately 50 mg of liver tissue and homogenized in anhydrous ethanol. Triglycerides (TG), high-density lipoprotein cholesterol (HDL-C), and low-density lipoprotein cholesterol (LDL-C) were measured using a biochemical analyzer (BMG, Germany).

2.6. Histological analysis

Liver tissue was removed from 20-week-old mice after a 4-hour fast. Tissue fixed in 4% paraformaldehyde for histological analysis or frozen in liquid nitrogen for storage. The paraffin sections were deparaffinized, rehydrated, and then stained with hematoxylin/eosin (Yuanye Bio-Technology, Shanghai, China) to visualize the morphology. Oil red O (ORO) staining (Solarbio, Beijing, China) was used to stain neutral TG and lipids in frozen sections. All sections were imaged with a light microscope (Olympus, Japan).

2.7. RNA-Sequencing (RNA-Seq)

Total RNA was isolated from livers using TRIzol reagent (Invitrogen, Carlsbad, CA, USA) and used as the template to construct cDNA libraries. RNA sequencing was performed with the liver sample from 20-week-old offspring. Sequencing was run on an Illumina system performed by Azenta Biotechnology (Soochow, China). Differentially expressed genes (DEGs) were determined by |foldchange| >1 and P values < 0.05. Volcano map, heat map and GSEA pathway enrichment analysis were performed. Images are plotted on the omicstudio Biology (website: https://www.omicstudio.cn/index). The genes enriched in GSEA were considered statistically significant when the nominal P-value was < 0.05 and |NES|>1.

2.8. Quantitative Real-Time PCR (qRT-PCR)

Total RNA was extracted using TRIzol reagent (Invitrogen, Carlsbad, CA, USA) and reverse transcribed using the RevertAid First Strand cDNA Synthesis Kit (K1622, Thermo Scientific, USA). The TB green Premix EX Taq kit (RR820A, TaKaRa, USA) was used for RT-qPCR. Real-time PCR reactions were performed on Bio-Rad iCycler iQ RT-qPCR machine. RNA concentration and quality were analyzed using NanoDrop2000. Gene expression was calculated using the $2^{-\Delta\Delta CT}$ method, and data were normalized to 18S or β-Actin. The primer sequences were provided in Additional file 1: Table S2.

2.9. Western blotting

Total protein was harvested from liver tissue, and cell line lysates using RIPA buffer (P0013B, Beyotime, China) supplemented with protease and phosphatase inhibitors (P001, NCM Beyotime, China). Protein concentrations were determined by the Bradford method (P0006, Beyotime, China). Samples were separated by SDS-PAGE and then transferred to polyvinyl difluoride (PVDF) membranes. Antibodies are listed in Additional file 1: Table S3. Primary antibodies were incubated overnight at 4°C, and secondary antibodies were incubated for 1 hour at room temperature. Visualization of signals using the enhanced chemiluminescence system (GE Healthcare, Piscataway, NJ, USA). Protein abundance was assessed by normalization to β-actin or α-Actinin.

2.10. Cell culture and transfection

HepG2 cells were obtained from ATCC in a medium supplemented with 10% FBS (Hyclone, Logan, UT, USA) and 1% penicillin-streptomycin (Hyclone, Logan, UT, USA), and all cell lines were maintained in an incubator containing 5% CO_2 at 37°C. Transfection was performed using 150 pmol of si-NC, si-GDF15, si-RGS16 (Gene Pharma, Shanghai, China) or 2μg pcDNA-empty, pcDNA-GDF15. GT-Transfect-Mate reagent (Gene Pharma, Shanghai, China) in Opti-MEM (Thermo Fisher Scientific, USA) was used, and the medium was exchanged after 8 hours of transfection. See Additional file 1: Table S4 for siRNA information. The pcDNA-GDF15 vector was constructed according to the sequence of GDF15 and the characteristics of the vector.

The sequence of the forward oligonucleotide is TAATACGACTCACTATAGGGCCACCATGCCCGGGCAAGAACTCAG; and the reverse oligonucleotide is TCTGAGATGAGTTTTTGTTCTATGCAGTGGCAGTCTTTGGCT.

2.11. Oil red staining of HepG2 cells

Lipid droplets were initially visualized and subsequently quantified by ORO staining (Solarbio, Beijing, China). After transfection for 24 h, the cells were fixed in 10% formalin for 30 min. The fixed cells were then stained in a pre-warmed ORO solution at 60°C for 30 min, and the red-stained lipid droplets were subsequently visualized using a light microscope. To quantify lipid accumulation, ORO was eluted with 100% isopropanol, and the OD of the eluate was measured using a biochemical analyzer (BMG, Germany). According to the manufacturer's instructions, TG levels in HepG2 cells were measured using the Triglyceride Quantification Kit (Jiancheng, Nanjing, China).

2.12. Statistical analysis

All data are shown as mean ± SEM. Statistical analysis was performed using t-test or two-way analysis of variance (ANOVA). The area under the curve (AUC) of glucose levels in GTT, ITT, and PTT was calculated using GraphPad Prism 9.0 (GraphPad Software, San Diego, CA). P-value < 0.05 was considered statistically significant.

3. Results

3.1. Distinct body weight trajectories in offspring

The number of litters was similar in both groups (CON: 161, IVF-ET: 133), and the sex ratio (female/male) was 1.1 (84:77) in the CON group and 1.0 (67:66) in the IVF group (Additional file 1: Table S2). The birth weights of both male and female offspring in the IVF-ET group were higher than those in the CON group at postnatal day 1 (Fig. 1a,1d); There was no significant difference in body weight at four weeks; however, the weights of male IVF-ET offspring showed an upward trend at eight weeks. At ten weeks, the male mice had significantly increased body weight compared to CON, while female offspring did not gain

weight rapidly until 18 weeks (Fig. 1b, 1e). To exclude nutritional effects, the daily intakes of the two groups were calculated, and no significant differences were found between the experimental and control groups (Fig. 1c, 1f). These results suggested that the IVF-ET procedure affects the normal development of offspring in mice.

3.2. Abnormal glucose metabolism in IVF-ET offspring

To further investigate the effects of IVF-ET on glucose homeostasis in the offspring, we performed the glucose tolerance test (GTT), insulin tolerance test (ITT), and pyruvate tolerance test (PTT) in male and female offspring of the IVF-ET and CON groups. For the male offspring, the area under the curve (AUC) of GTT, ITT, and PTT was increased in the IVF-ET group (Fig. 2a, 2c); Glucose homeostasis was disturbed in the IVF-ET group at 15, 30, and 90 minutes after glucose injection compared to the CON group (Fig. 2a); ITT results showed higher blood glucose in the IVF-ET group at 0, 15, 30, and 60 minutes, indicating decreased insulin sensitivity (Fig. 2b); Despite slight differences in fasting blood glucose, there was no significant difference in blood glucose levels between the two groups after pyruvate injection (Fig. 2c). However, for the female offspring, there were no significant differences in fasting glucose, GTT and PTT tests between the two groups, as was the area under their curves (Fig. 2d, 2f), and the ITT test showed differences in blood glucose at 0 and 15 minutes after insulin injection and a higher AUC in the IVF-ET group than in the CON group (Fig. 2e), suggesting slight insulin resistance.

3.3. Abnormal lipid metabolism in IVF-ET male offspring

The above results indicate that IVF-ET male offspring exhibit more severely impaired glucose metabolism than females. Compared to the CON group, IVF-ET male offspring showed significant weight gain at eight weeks of age that persisted until 28 weeks, whereas IVF-ET female offspring showed insignificant weight changes by 18 weeks of age compared to the CON group. Therefore, in combination with bodyweight data and glucose metabolism phenotypes, male offspring were chosen as the main subjects in this study. At 20 weeks, we measured the weight of organs associated with metabolisms, such as the liver, brain, spleen, heart, kidney, subcutaneous white adipose tissue (sWAT), epididymal white adipose tissue (eWAT), and interscapular brown adipose tissue (iBAT), and calculated the relative organ weight/body weight ratio of male offspring. Both liver and eWAT weight were found to be increased, while only the ratio of epididymal fat weight/body weight, but not liver, was significantly increased (Fig. 3b, 3c). Liver tissue is not only the most critical organ in which glucose metabolism occurs but also the most critical organ in regulating lipid metabolism in the organism [22, 23]. Then we performed a histological analysis of the liver. HE staining showed that hepatocytes in the IVF-ET male offspring had extensive steatosis, ballooning degeneration, and a scattered infiltration of a small number of inflammatory cells compared to controls (Fig. 3a). Oil red O staining showed significant lipid deposition in IVF-ET male offspring liver tissue (Fig. 3a). Lipid metabolism analysis using plasma and liver tissue showed significantly increased plasma triglycerides and LDL-C and decreased HDL-C in the IVF-ET male offspring (Fig. 3d-3f); consistent results were also found in liver tissues (Fig. 3g-3i). It can be inferred that the offspring of IVF-ET males have abnormal lipid metabolism.

3.4. Altered liver transcriptome in IVF-ET male offspring

To explore the underlying mechanisms of the lipid metabolism in male offspring conceived by IVF-ET, we performed the RNA-sequencing of livers from both groups. Fifty-nine genes were upregulated, and seventy-six genes were downregulated in the IVF-ET group compared to the CON group (Fig. 4a). A heat map of metabolism-related genes was generated (Fig. 4b). After a pairwise comparison of GSEA, it was revealed that many genes involved in the initial fatty acid synthesis process were significantly upregulated in the GO and KEGG enrichment pathways in the IVF-ET group compared to the CON group (Fig. 4c, 4d).

We verified the sequencing results by RT-qPCR and confirmed the upregulation of many genes related to lipid synthesis, such as *Pparg*, *Srebf1*, *Dgat2*, *Cebpb*, and *Fabp2* (Fig. 4e). No significant changes were observed for several genes related to fatty acid oxidation, such as *Ppara*, *Pgc1a*, and *Acox1* (Fig. 4f). All data suggest that abnormal liver lipid metabolism in IVF-ET male offspring mice may be primarily related to the lipid synthesis pathway.

3.5. Decreased GDF15 and increased RGS16 were found in the liver of IVF-ET offspring

Gdf15 plays a vital role in obesity and related metabolic diseases [24, 25]. *Rgs16* provides a signaling mechanism for glucose production to inhibit G protein-coupled receptors (GPCR) -stimulated fatty acid oxidation in hepatocytes [26]. Both of which are implicated in hepatic lipid metabolism. In RNA-sequencing results, we found that the expression of *Gdf15* and *Rgs16* in liver tissues in the IVF-ET group was significantly different by more than 2-fold compared to the CON group (Fig. 4a, 4b). Validation of the expression of these two genes in mouse liver tissue by q-PCR revealed reduced *Gdf15* (Fig. 5a) and increased *Rgs16* (Fig. 5b), which is consistent with the results of the RNA-Seq data. Western blotting results confirmed that protein changes of both GDF15 and RGS16 were consistent with mRNA expression studies (Fig. 5c).

3.6 Increased phosphorylation of AKT and ERK1/2 in the liver of IVF-ET offspring

It is known that GDF15 can activate the downstream AKT and ERK1/2 pathways, which contribute to the regulation of hepatic mitochondrial function and energy metabolism. Therefore, we continued to check if the downstream of GDF15 had been affected. We verified the expression of ERK1/2, AKT, p-ERK1/2, and p-AKT levels in the liver of IVF-ET male offspring by Western blot and found that the expression of p-ERK1/2 and p-AKT was reduced in the liver of IVF-ET male offspring mice (Fig. 5c). It is suggested that the impaired lipid metabolism in the IVF-ET group may be due to abnormalities in the ERK1/2 and AKT pathways.

3.7. GDF15 negatively regulated RGS16 in lipid deposition in hepatocytes

To investigate the relationship between GDF15, RGS16, and liver lipid metabolism, we performed RNA interference to knock down GDF15 expression in HepG2 cells *in vitro*. Interestingly, we found that knockdown of GDF15 was followed by an increase in the expression of RGS16 (Fig. 6a, 6b). De novo lipid synthesis genes such as *PPARG*, *SREBF1*, *FABP2*, *CEBPB*, and *FABP2* were increased, while no significant changes were found in fatty acid oxidation genes (Fig. 6c); Phosphorylation of ERK1/2 and AKT levels were significantly decreased (Fig. 6b). Furthermore, we overexpressed GDF15 by transfecting HepG2 cells with GDF15 containing pcDNA3.1-myc-His plasmids. Interestingly, we found that overexpression of GDF15 was followed by a significant decrease in RGS16 mRNA and protein expression (Fig. 6d, 6e). The expression of lipogenic genes *SREBF1* and *FABP2* was decreased, while the expression of fatty acid oxidation genes *PPARA* and *ACOX1* was increased (Fig. 6f). Phosphorylation of ERK1/2 and AKT were significantly increased (Fig. 6e). Our findings indicated that a negative regulatory relationship between GDF15 and RGS16 may cause changes in mRNA levels of lipogenic and fatty acid oxidation genes by affecting the phosphorylation of ERK1/2 and AKT, leading to increased lipid deposition.

3.8. Knockdown of RGS16 reverses GDF15 downregulatin-induced lipid deposition

Since decreased GDF15 results in abnormal lipid metabolism and increased expression of RGS16, we wondered if reducing RGS16 could rescue the phenotypes caused by GDF15 down-regulation.

By RGS16 RNAi in HepG2 cells, we found that reduced RGS16 mRNA expression was followed by reduced levels of lipogenic genes *PPARG*, *SREBF1*, and *FABP2* mRNA, increased expression of fatty acid oxidation gene *PGC1A* (Supplementary Fig. S1b) and increased phosphorylation of ERK1/2 and AKT (Supplementary Fig. S1a), suggesting that a reduction in RGS16 may increase fatty acid oxidation and inhibit initial lipid synthesis, resulting in reduced lipid deposition in hepatocytes.

We then knockdown of GDF15 and RGS16 expression simultaneously to see if it could reverse the abnormal lipid deposition caused by GDF15 downregulation in hepatocytes. The cell oil red O staining showed that knockdown of RGS16 reversed the increased lipid deposition (Fig. 7a), altered mRNA expression of lipogenic and fatty acid oxidation genes (Fig. 7b), and phosphorylation of ERK1/2 and AKT caused by GDF15 knockdown (Fig. 7c). These results suggested that the knockdown of RGS16 in HepG2 cells reversed the abnormal lipid deposition induced by GDF15 knockdown.

4. Discussion

The embryonic and fetal developments are susceptible to environmental factors, and any sub-optimal conditions during the development stages of gametes, embryos, and the fetus could affect the health of the offspring after birth, which is known as the “embryo-fetal origin of disease” theory [27]. A vast body of

evidence suggests that children conceived by IVF-ET may be at increased risk of chronic diseases [8, 10]. In this study, increased body weight, abnormal glucose metabolism and lipid metabolism, particularly abnormal liver lipid deposition, were observed in IVF-ET male mice offspring. Sex-specific phenotypes, such as male offspring exhibiting more severely impaired glucose metabolism, insulin resistance, abnormal pyruvate tolerance, and earlier weight gain than females, were found in our study. It was evident that there may be gender differences in the effects of IVF-ET on offspring. To date, various metabolic phenotypes of IVF-ET offspring have been reported. Lower birth weight [28] and catch-up growth [15, 29], normal birth weight [17], and higher body weight as found in our study, were observed. IVF-ET offspring could present with impaired glucose metabolism, insulin resistance, and abnormal pyruvate tolerance after receiving a high-fat diet [20]; Severe glucose metabolism dysfunction sometimes occurs only in female offspring and sometimes only in male offspring [15, 16, 18, 29]. We presumed that the sex-specific phenotypes might be caused by different mouse strains, culture media, breeding conditions [17], as well as female estrogenic protection and epigenetic modifications of imprinted genes [30].

Moreover, we found increased body fat and liver weight, abnormal liver steatosis and lipid deposition, higher TG/LDL-C, and lower HDL-C in the male IVF-ET offspring at 22 weeks. These findings suggest abnormal lipid metabolism in IVF-ET male mice. It is well known that hepatic lipid metabolism plays a key role with essential functions in the de novo synthesis of fatty acids and ketogenesis [31]. Therefore, we have sequenced the liver transcriptome and carried out an in-depth study of the possible mechanisms underlying the abnormalities in lipid metabolism. GO, and KEGG enrichment analysis results revealed an upregulated transcriptional status of genes involved in the primary synthesis of hepatic lipids in the livers of IVF-ET mice compared to CON mice. It suggests that the mechanism of increased hepatic lipid deposition in IVF-ET male offspring may be related to abnormalities in pathways related to lipid synthesis. It is well known that hyperglycemia, insulin resistance, hypertriglyceridemia, and abnormal fatty deposits in the liver are the main features of Non-alcoholic fatty liver disease (NAFLD) and other metabolic syndromes. Therefore, we speculate that IVF-ET conceived male mice might be susceptible to metabolic disorders relative to NAFLD.

Previous studies have shown that increased phosphorylation of insulin receptors AKT and ERK1/2 contributes to the regulation of hepatic mitochondrial function and energy metabolism [32–35]. Growth differentiation factor 15 (GDF15), a member of the transforming growth factor-β superfamily, is abundantly expressed in placental trophoblast cells during gestation and is synthesized and secreted mainly in the liver, where it is involved in various biological processes, including energy balance, body weight regulation and cachexia due to cancer and chronic diseases [36, 37]. It can promote fatty acid oxidation and inhibit lipid de novo synthesis in hepatocytes by binding to the GFRAL-RET receptor on the surface of target cells, leading to activation of the downstream AKT and ERK1/2 pathways [38]. G protein signaling regulator 16 (RGS16) was initially cloned from the retina [39], which expressions in the heart, liver, hematopoietic cells, and brain [40, 41]. RGS16 is involved in adaptive immunity, platelet migration, and glucose or fat metabolism. High expression of RGS16 leads to hepatic steatosis, reduced blood glucose and β-ketone levels, and decreased gene expression for fatty acid oxidation in the liver; In

contrast, *Rgs16* KO mice exhibited the opposite phenotype as elevated expression of fatty acid oxidation genes in the liver, higher rates of fatty acid oxidation in liver extracts, and higher plasma β-ketone levels [26, 42]. In IVF-ET mice, we found increased expression of RGS16, downregulation of GDF15, p-ERK1/2, and p-AKT, and increased expression of lipogenic genes in the livers of IVF-ET male offspring. We, therefore, deduced that abnormal lipid metabolism in IVF-ET male offspring might be associated with abnormal GDF15-RGS16-p-ERK1/2/p-AKT pathway. Combining the known opposite functions reported with GDF15/RGS16 and the opposite expression found in our studies, we presumed that there might be a negative relationship between these two genes. However, no studies have shown an association between GDF15 and RGS16.

In vitro in HepG2 cells, knockdown of GDF15 resulted in abnormal upregulated expression of RGS16, inhibition of the phosphorylation of ERK1/2 and AKT, elevated expression of lipogenic genes, decreased expression of fatty acid oxidation genes, and increased cellular lipid deposition. Overexpression of GDF15 reduced the expression of RGS16, and subsequently increased the phosphorylation of ERK1/2 and AKT, reduced the expression of lipogenic genes, and increased the expression of fatty acid oxidation genes. These findings suggest that there may be a negative regulation between GDF15 and RGS16. Therefore, we speculate that RGS16 negatively regulated by GDF15 could be a possible mechanism for the abnormal lipid metabolism phenotype in IVF-ET male mice and may be an effective way to improve the metabolic abnormalities in IVF-ET offspring. Nevertheless, this is an *in vitro* cell experiment and might not fully explain the lipid metabolism pathway of IVF-ET offspring.

However, the factors affecting the reduced hepatic GDF15 expression in their offspring remain to be investigated, and epigenetic changes or intergenerational inheritance may be a potential and valid explanation [43, 44]. When genome-wide epigenetic reprogramming occurs, the fertilization and pre-implantation stages are critical periods of development. Manipulations during *in vitro* fertilization and *in vitro* culture of fertilized eggs may lead to oxidative stress in fertilized egg cells, affecting cell division, among other things [45]. ROS (reactive oxygen species, superoxide, and hydrogen peroxide) produced by oxidative stress have been shown to regulate major epigenetic processes, DNA methylation, and histone acetylation [46]. The abnormal epigenetic modifications may also be associated with direct, intergenerational, and transgenerational effects in offspring [47].

In summary, the IVF-ET model in this study eliminates the genetic diversity and complex environmental background of humans and is used to demonstrate that *in vitro* fertilization-embryo transfer can have long-term effects on the growth and glucolipid metabolism in offspring. Inhibiting RGS16 expression could reverse the abnormal lipid metabolism caused by GDF15 under-expression, which may be an effective way to alleviate abnormal lipid metabolism in the offspring of IVF-ET males. However, our findings may not be directly applicable to humans due to the complex human genetic background, hormonal environment, and application of various ovulation drugs in humans. Still, it provides valuable information for prevention and clinical decision-making.

5. Conclusion

Male mice born via IVF-ET exhibit a higher risk of glucolipid metabolism manifested as increased body weight, abnormal GTT, ITT, PTT, and abnormal liver lipid deposition. GDF15-RGS16-p-ERK1/2/p-AKT may be the underlying mechanism for lipid metabolism. Realizing the health problems of ART offspring in the long term will help improve the IVF-ET technique to be more optimized to reduce unnecessary adverse effects. This study is only a step in that direction, and more work is needed.

Abbreviations

ART	Assisted reproductive technology
CON	Control group
AI	Artificial insemination
IVF-ET	In vitro fertilization and embryo transfer
ACh	Acetylcholine
GTT	Glucose tolerance test
ITT	Insulin tolerance test
PTT	Pyruvate tolerance test
TG	Triglycerides
LDL-C	Low-density lipoprotein cholesterol
HDL-C	High-density lipoprotein cholesterol
sWAT	Subcutaneous white adipose tissue
eWAT	Epididymal white adipose tissue
iBAT	Interscapular brown adipose tissue
FBS	Fetal bovine serum
CO_2	Carbon dioxide
ORO	Oil red O
RT-qPCR	Reverse transcription polymerase chain reaction
RNA-Seq	RNA sequencing
RNAi	RNA interference
PVDF	PolyVinylideneFluoride
Gdf15	Growth differentiation factor 15
Rgs16	Regulator of G protein signaling 16
PMSG	Pregnant mare serum gonadotropin
HCG	Human chorionic gonadotropin
HTF	Human tubal fluid medium
KSOM	Potassium simplex optimized medium
DEG	Differentially expressed gene
GSEA	Gene set enrichment analysis

GO	Gene ontology
KEGG	Kyoto encyclopedia of genes and genomes
NES	Enrichment score
ERK	Extracellular-signal-regulated kinase
AKT (PKB)	Protein kinase B
GPCR	G protein-coupled receptors
Pparg	Peroxisome proliferator-activated receptor gamma
Srebf1	Sterol regulatory element binding protein 1
Dgat2	Diacylglycerol acyltransferase 2
Cebpb	CCAAT/enhancer-binding protein beta
Fabp2	Fatty acid-binding protein 2
Ppara	Peroxisome proliferator-activated receptor alpha
Pgc1a	Peroxisome proliferator activated receptor coactivator-1 alpha
Acox1	Acyl-CoA oxidase 1
NAFLD	Non-alcoholic fatty liver disease
SEM	Standard error of the means
ns	Not significant

Declarations

Authors' contributions:

JL and YZ processed the data and figures, and drafted the manuscript; YZ generated the animal models; JL and DZ performed the molecular studies; YS and LL performed the glucose metabolism experiments; LL and WL performed the cellular experiments; BW, HY and XZ performed the construction of recombinant plasmids. The work was supervised by MS. All authors read and approved the final manuscript.

Funding:

National Key R&D Program of China (2019YFA0802600); National Natural Science Foundation of China (81974244, 81570960); Jiangsu Province's Key Discipline of Prenatal Diagnosis (FXK201746).

Availability of data and materials:

The data used in this study are available from the corresponding author on reasonable request.

Ethics approval and consent to participate

The animal study was reviewed and approved by Jiangsu Model Organisms Center's Ethical Committee in Animal Research.

Consent for publication

All authors agree to the content of the manuscript and consent to its publication.

Competing interests

The authors declare that they have no competing interests.

Acknowledgments

Not applicable.

Footnotes:

Publisher's Note

Springer Nature remains neutral with regard to jurisdictional claims in published maps and institutional affiliations.

Jingliu Liu and Yichen Zhu contributed equally to this work.

Contributor Information:

Miao Sun, Email: miaosunsuda@163.com .

References

1. Bai, F. *et al.* Assisted reproductive technology service availability, efficacy and safety in mainland China: 2016. Hum Reprod **35**, 446–452, doi:10.1093/humrep/dez245 (2020).
2. Pourakbari, R., Ahmadi, H., Yousefi, M. & Aghebati-Maleki, L. Cell therapy in female infertility-related diseases: Emphasis on recurrent miscarriage and repeated implantation failure. Life Sci **258**, 118181, doi:10.1016/j.lfs.2020.118181 (2020).
3. Tarín, J. J., García-Pérez, M. A. & Cano, A. Assisted reproductive technology results: why are live-birth percentages so low? Mol Reprod Dev **81**, 568–583, doi:10.1002/mrd.22340 (2014).
4. Fleming, T. P., Velazquez, M. A. & Eckert, J. J. Embryos, DOHaD and David Barker. J Dev Orig Health Dis **6**, 377–383, doi:10.1017/s2040174415001105 (2015).
5. Duranthon, V. & Chavatte-Palmer, P. Long term effects of ART: What do animals tell us? Mol Reprod Dev **85**, 348–368, doi:10.1002/mrd.22970 (2018).

6. Basatemur, E. & Sutcliffe, A. Follow-up of children born after ART. *Placenta* **29 Suppl B**, 135–140, doi:10.1016/j.placenta.2008.08.013 (2008).
7. Chen, M., Norman, R. J. & Heilbronn, L. K. Does in vitro fertilisation increase type 2 diabetes and cardiovascular risk? Curr Diabetes Rev **7**, 426–432, doi:10.2174/157339911797579151 (2011).
8. Ceelen, M., van Weissenbruch, M. M., Vermeiden, J. P., van Leeuwen, F. E. & Delemarre-van de Waal, H. A. Cardiometabolic differences in children born after in vitro fertilization: follow-up study. J Clin Endocrinol Metab **93**, 1682–1688, doi:10.1210/jc.2007-2432 (2008).
9. Scherrer, U. *et al.* Systemic and pulmonary vascular dysfunction in children conceived by assisted reproductive technologies. Circulation **125**, 1890–1896, doi:10.1161/circulationaha.111.071183 (2012).
10. Sakka, S. D. *et al.* Absence of insulin resistance and low-grade inflammation despite early metabolic syndrome manifestations in children born after in vitro fertilization. Fertil Steril **94**, 1693–1699, doi:10.1016/j.fertnstert.2009.09.049 (2010).
11. Järvisalo, M. J. *et al.* Increased aortic intima-media thickness: a marker of preclinical atherosclerosis in high-risk children. Circulation **104**, 2943–2947, doi:10.1161/hc4901.100522 (2001).
12. Rexhaj, E. *et al.* Mice generated by in vitro fertilization exhibit vascular dysfunction and shortened life span. J Clin Invest **123**, 5052–5060, doi:10.1172/jci68943 (2013).
13. Shi, Y. *et al.* Methylation-reprogrammed CHRM3 results in vascular dysfunction in the human umbilical vein following IVF-ET. Biol Reprod, doi:10.1093/biolre/ioab234 (2021).
14. Zhang, M. *et al.* Methylation-reprogrammed AGTR1 results in increased vasoconstriction by angiotensin II in human umbilical cord vessel following in vitro fertilization-embryo transfer. Life Sci **234**, 116792, doi:10.1016/j.lfs.2019.116792 (2019).
15. Feuer, S. K. *et al.* Use of a mouse in vitro fertilization model to understand the developmental origins of health and disease hypothesis. Endocrinology **155**, 1956–1969, doi:10.1210/en.2013-2081 (2014).
16. Scott, K. A. *et al.* Glucose parameters are altered in mouse offspring produced by assisted reproductive technologies and somatic cell nuclear transfer. Biol Reprod **83**, 220–227, doi:10.1095/biolreprod.109.082826 (2010).
17. Donjacour, A., Liu, X., Lin, W., Simbulan, R. & Rinaudo, P. F. In vitro fertilization affects growth and glucose metabolism in a sex-specific manner in an outbred mouse model. Biol Reprod **90**, 80, doi:10.1095/biolreprod.113.113134 (2014).
18. Calle, A. *et al.* Male mice produced by in vitro culture have reduced fertility and transmit organomegaly and glucose intolerance to their male offspring. Biol Reprod **87**, 34, doi:10.1095/biolreprod.112.100743 (2012).
19. Qin, N. *et al.* Abnormal Glucose Metabolism in Male Mice Offspring Conceived by in vitro Fertilization and Frozen-Thawed Embryo Transfer. Front Cell Dev Biol **9**, 637781, doi:10.3389/fcell.2021.637781 (2021).

20. Narapareddy, L. *et al.* Sex-specific effects of in vitro fertilization on adult metabolic outcomes and hepatic transcriptome and proteome in mouse. Faseb j **35**, e21523, doi:10.1096/fj.202002744R (2021).
21. Wang, L. Y. *et al.* Alteration of fatty acid metabolism in the liver, adipose tissue, and testis of male mice conceived through assisted reproductive technologies: fatty acid metabolism in ART mice. Lipids Health Dis **12**, 5, doi:10.1186/1476-511x-12-5 (2013).
22. Jones, J. G. Hepatic glucose and lipid metabolism. Diabetologia **59**, 1098–1103, doi:10.1007/s00125-016-3940-5 (2016).
23. Trefts, E., Gannon, M. & Wasserman, D. H. The liver. Curr Biol **27**, R1147-r1151, doi:10.1016/j.cub.2017.09.019 (2017).
24. Wang, D. *et al.* GDF15: emerging biology and therapeutic applications for obesity and cardiometabolic disease. Nat Rev Endocrinol **17**, 592–607, doi:10.1038/s41574-021-00529-7 (2021).
25. Kim, J. M. *et al.* NAG-1/GDF15 transgenic mouse has less white adipose tissue and a reduced inflammatory response. *Mediators Inflamm* 2013, 641851, doi:10.1155/2013/641851 (2013).
26. Pashkov, V. *et al.* Regulator of G protein signaling (RGS16) inhibits hepatic fatty acid oxidation in a carbohydrate response element-binding protein (ChREBP)-dependent manner. J Biol Chem **286**, 15116–15125, doi:10.1074/jbc.M110.216234 (2011).
27. Zou, K., Ding, G. & Huang, H. Advances in research into gamete and embryo-fetal origins of adult diseases. Sci China Life Sci **62**, 360–368, doi:10.1007/s11427-018-9427-4 (2019).
28. Qin, J., Liu, X., Sheng, X., Wang, H. & Gao, S. Assisted reproductive technology and the risk of pregnancy-related complications and adverse pregnancy outcomes in singleton pregnancies: a meta-analysis of cohort studies. Fertil Steril **105**, 73–85.e71-76, doi:10.1016/j.fertnstert.2015.09.007 (2016).
29. Chen, M. *et al.* Altered glucose metabolism in mouse and humans conceived by IVF. Diabetes **63**, 3189–3198, doi:10.2337/db14-0103 (2014).
30. Lazaraviciute, G., Kauser, M., Bhattacharya, S., Haggarty, P. & Bhattacharya, S. A systematic review and meta-analysis of DNA methylation levels and imprinting disorders in children conceived by IVF/ICSI compared with children conceived spontaneously. Hum Reprod Update **20**, 840–852, doi:10.1093/humupd/dmu033 (2014).
31. Alves-Bezerra, M. & Cohen, D. E. Triglyceride Metabolism in the Liver. Compr Physiol **8**, 1–8, doi:10.1002/cphy.c170012 (2017).
32. Zhang, M., Pan, J. & Huang, P. Interaction between RAS gene and lipid metabolism in cancer. Zhejiang Da Xue Xue Bao Yi Xue Ban **50**, 17–22, doi:10.3724/zdxbyxb-2021-0054 (2021).
33. Wang, X. *et al.* 2,3,5,4'-tetrahydroxystilbene-2-O-β-D-glucoside induces autophagy of liver by activating PI3K/Akt and Erk pathway in prediabetic rats. BMC Complement Med Ther **20**, 177, doi:10.1186/s12906-020-02949-w (2020).
34. Rebollo-Hernanz, M., Aguilera, Y., Martin-Cabrejas, M. A. & Gonzalez de Mejia, E. Phytochemicals from the Cocoa Shell Modulate Mitochondrial Function, Lipid and Glucose Metabolism in Hepatocytes via

Activation of FGF21/ERK, AKT, and mTOR Pathways. Antioxidants (Basel) **11**, doi:10.3390/antiox11010136 (2022).

35. Hagiwara, A. *et al.* Hepatic mTORC2 activates glycolysis and lipogenesis through Akt, glucokinase, and SREBP1c. Cell Metab **15**, 725–738, doi:10.1016/j.cmet.2012.03.015 (2012).
36. Sheka, A. C. *et al.* Nonalcoholic Steatohepatitis: A Review. Jama **323**, 1175–1183, doi:10.1001/jama.2020.2298 (2020).
37. Bootcov, M. R. *et al.* MIC-1, a novel macrophage inhibitory cytokine, is a divergent member of the TGF-beta superfamily. Proc Natl Acad Sci U S A **94**, 11514–11519, doi:10.1073/pnas.94.21.11514 (1997).
38. Zhang, Z. *et al.* ARRB1 inhibits non-alcoholic steatohepatitis progression by promoting GDF15 maturation. J Hepatol **72**, 976–989, doi:10.1016/j.jhep.2019.12.004 (2020).
39. Chen, C. K., Wieland, T. & Simon, M. I. RGS-r, a retinal specific RGS protein, binds an intermediate conformation of transducin and enhances recycling. Proc Natl Acad Sci U S A **93**, 12885–12889, doi:10.1073/pnas.93.23.12885 (1996).
40. Patten, M. *et al.* Endotoxin induces desensitization of cardiac endothelin-1 receptor signaling by increased expression of RGS4 and RGS16. Cardiovasc Res **53**, 156–164, doi:10.1016/s0008-6363(01)00443-6 (2002).
41. Kim, K., Lee, J. & Ghil, S. The regulators of G protein signaling RGS16 and RGS18 inhibit protease-activated receptor 2/Gi/o signaling through distinct interactions with Gα in live cells. FEBS Lett **592**, 3126–3138, doi:10.1002/1873-3468.13220 (2018).
42. Zhang, Y. *et al.* Hepatic arginase 2 (Arg2) is sufficient to convey the therapeutic metabolic effects of fasting. Nat Commun **10**, 1587, doi:10.1038/s41467-019-09642-8 (2019).
43. Lira-Albarrán, S., Liu, X., Lee, S. H. & Rinaudo, P. DNA methylation profile of liver of mice conceived by in vitro fertilization. J Dev Orig Health Dis, 1–9, doi:10.1017/s2040174421000313 (2021).
44. Hanna, C. W., Demond, H. & Kelsey, G. Epigenetic regulation in development: is the mouse a good model for the human? Hum Reprod Update **24**, 556–576, doi:10.1093/humupd/dmy021 (2018).
45. Wojsiat, J., Korczyński, J., Borowiecka, M. & Żbikowska, H. M. The role of oxidative stress in female infertility and in vitro fertilization. Postepy Hig Med Dosw (Online) **71**, 359–366, doi:10.5604/01.3001.0010.3820 (2017).
46. Hayes, P. & Knaus, U. G. Balancing reactive oxygen species in the epigenome: NADPH oxidases as target and perpetrator. Antioxid Redox Signal **18**, 1937–1945, doi:10.1089/ars.2012.4895 (2013).
47. Ben Maamar, M., Nilsson, E. E. & Skinner, M. K. Epigenetic transgenerational inheritance, gametogenesis and germline development†. Biol Reprod **105**, 570–592, doi:10.1093/biolre/ioab085 (2021).

Figures

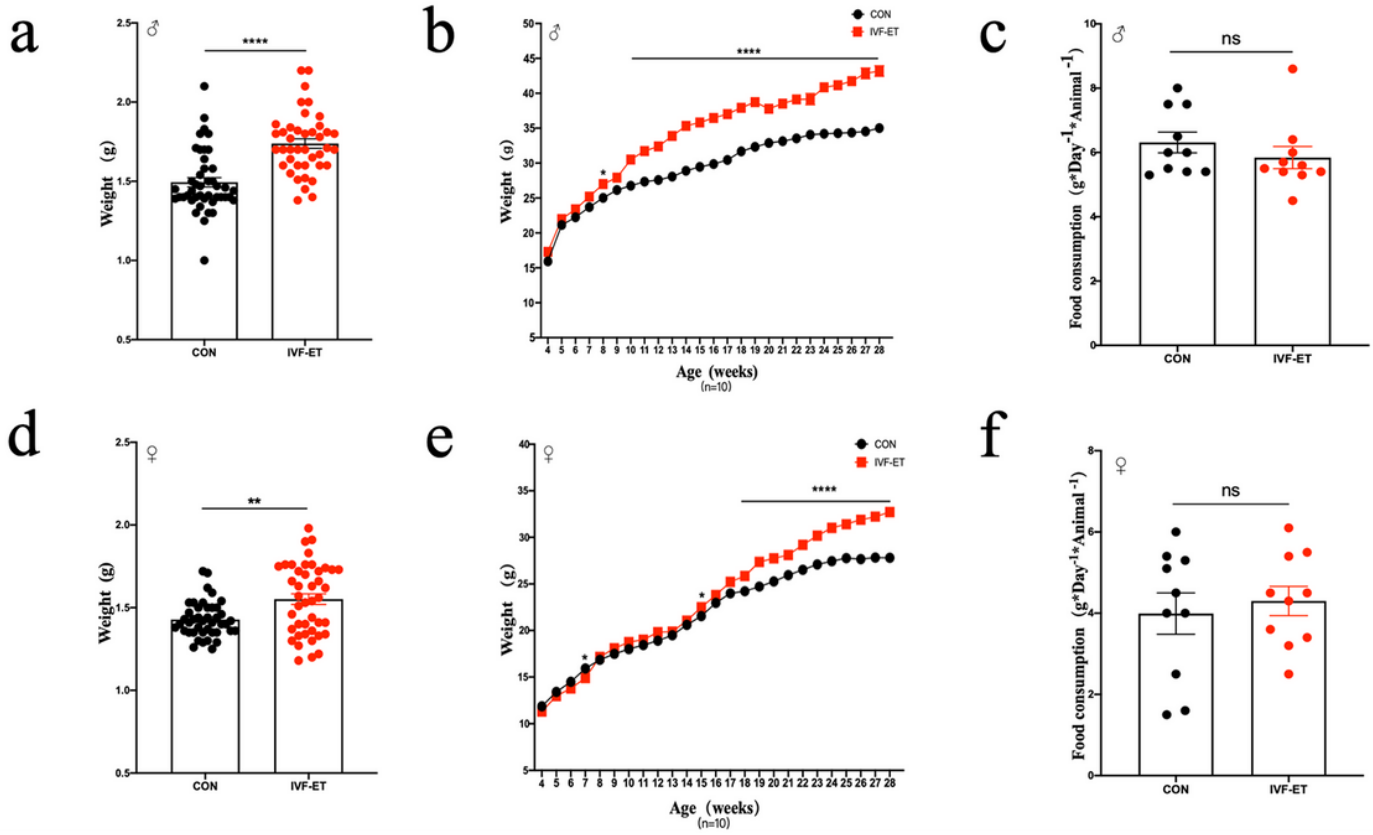

Figure 1

Birth weights, growth charts, and food intake of offspring. **a.** Birthweights of male offspring (CON: n=44; IVF-ET: n=42). **b.** Growth curves of male offspring after weaning (CON: n=10; IVF-ET: n=10). **c.** Food intake in male offspring (CON: n=10; IVF-ET: n=10). **d.** Birthweights of female offspring (CON: n=43; IVF-ET: n=43). **e.** Growth curves of female offspring after weaning (CON: n=10; IVF-ET: n=10). **f.** Food intake in female offspring (CON: n=10; IVF-ET: n=10). For bar graphs, data represent mean+SEM. Symbols under curves: ♂, male; ♀, female; *, p<0.05; **, p<0.01; ****, p<0.001; ns, not significant. Significance was determined by 2-tailed unpaired t-test in a, c, d, and f, and 2-way ANOVA in b and c.

Figure 2

GTT, ITT and PTT in offspring. **a.** Glucose tolerance test and AUC in male offspring (CON: n=10; VF-ET: n=7). **b.** Insulin tolerance test and AUC in male offspring (CON: n=9; IVF-ET: n=7). **c.** Pyruvate tolerance test and AUC in male offspring (CON: n=9; IVF-ET: n=7). **d.** Glucose tolerance test and AUC in female offspring (CON: n=7; VF-ET: n=7). **e.** Insulin tolerance test and AUC in female offspring (CON: n=8; IVF-ET: n=8). **f.** Pyruvate tolerance test and AUC in female offspring (CON: n=8; IVF-ET: n=8). For bar graphs, data

represent mean+SEM. ♂, male; ♀, female; *, p<0.05; **, p<0.01; ***, p<0.001; ns, not significant. Relative to control, by ANOVA.

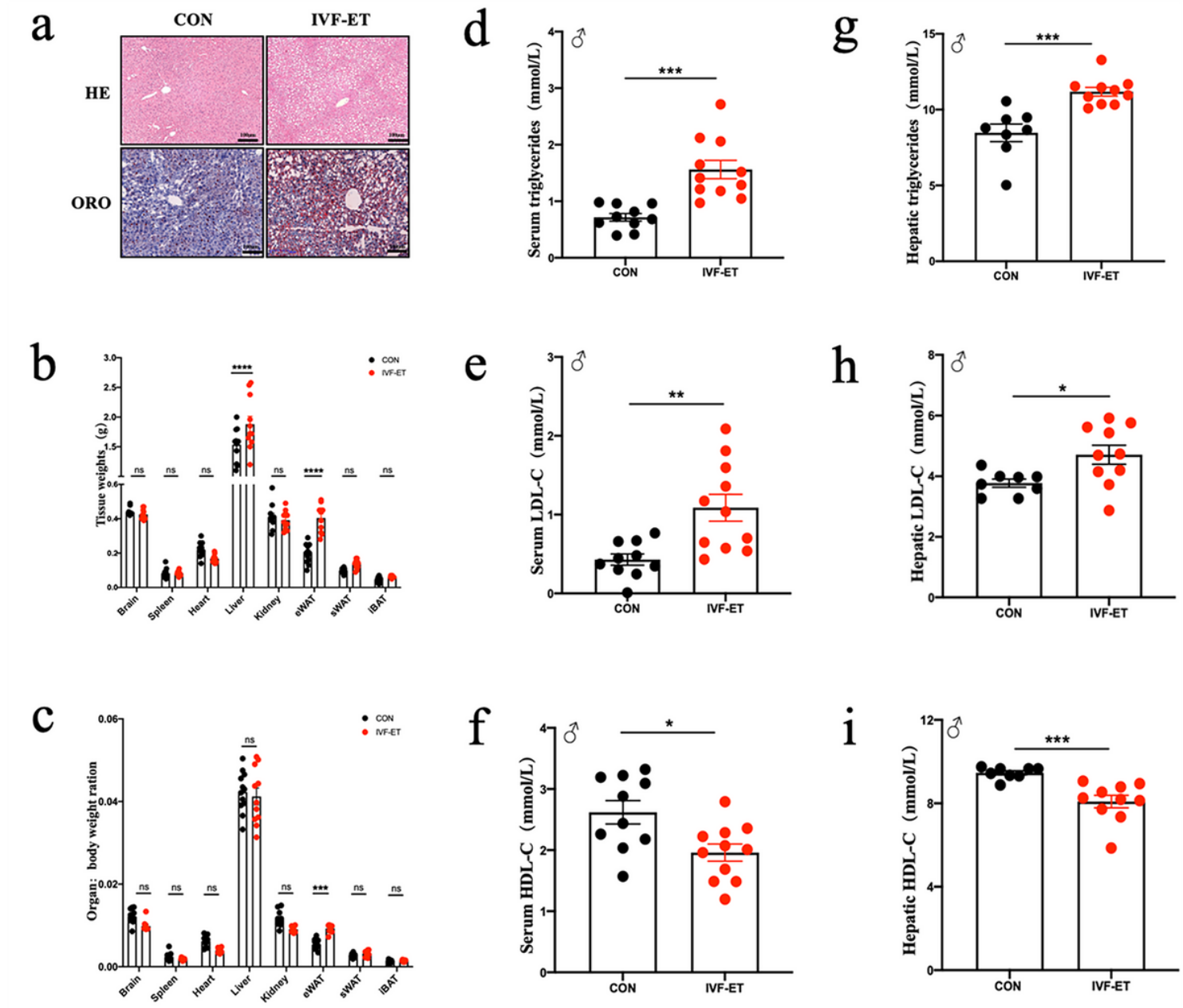

Figure 3

Analysis of liver and lipid metabolism factors in male offspring. **a.** HE staining and oil-red O staining of liver tissue (scale bar=100μm). **b.** Weight of multiple organs of male offspring (CON: n=12; IVF-ET: n=11). **c.** The proportion of each organ to body weight (CON: n=12; IVF-ET: n=11). **d-f.** Plasma levels of Triglycerides, LDL-C, HDL-C (CON: n=10; IVF-ET: n=11). **g-i.** Triglycerides, LDL-C, HDL-C levels in liver tissue (CON: n=8; IVF-ET: n=10). TG, triacylglycerol; HDL-C, high-density lipoprotein cholesterol; LDL-C, low-density lipoprotein cholesterol. For bar graphs, data represent mean+SEM. *, p<0.05; ** p<0.01; ***, p<0.001; ****, p<0.001; ns, not significant. Relative to control, by two-tailed Student's t-test.

Figure 4

Transcriptome analysis in livers of IVF-ET male offspring. **a.** Volcano plot demonstrating significantly altered genes by expression level and P-value. *Rgs16* and *Gdf15* are highlighted as highly regulated genes identified within the dataset; **b.** Heat map of differential genes associated with lipid metabolism; **c.** Enrichment map of genes involved in processes related to fatty acid metabolism; **d.** Enrichment map of genes involved in pathways related to unsaturated fatty acid metabolism. **e.** mRNA levels of genes related to the fatty acid synthesis pathway in liver tissue; **f.** mRNA levels of genes related to the fatty acid oxidation pathway in liver tissue. NES, Normalized enrichment score; GO, Gene Ontology; BP, Biological process; KEGG, Kyoto encyclopedia of genes and genomes (n=5 mice per group). For bar graphs, data represent mean+SEM. *, p<0.05; **, p<0.01; ***, p<0.001; ns, not significant. Relative to control, by two-tailed Student's t-test.

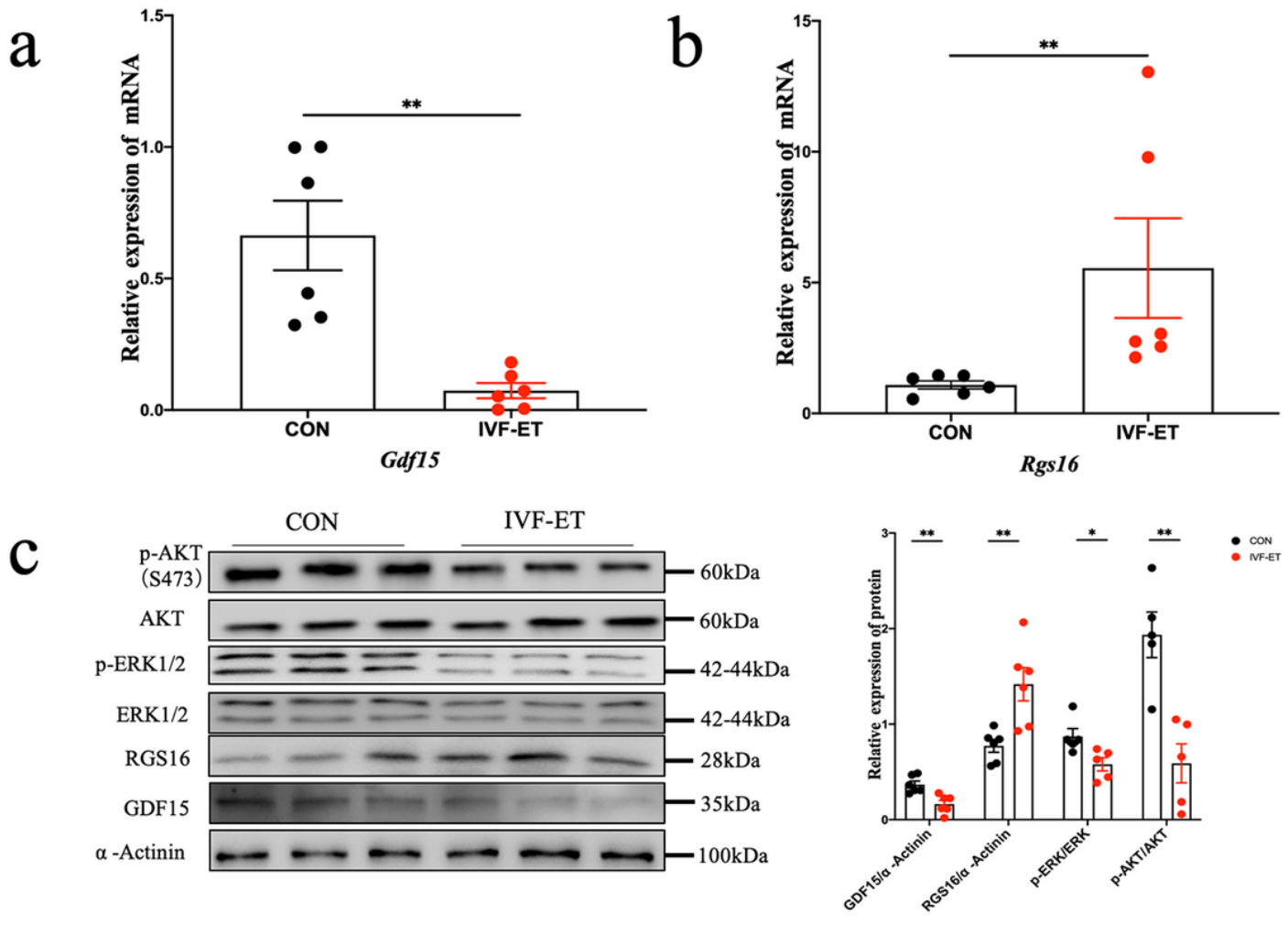

Figure 5

Expression of GDF15, RGS16, ERK1/2, AKT, and p-AKT **a.** Expression levels of *Gdf15* mRNA in liver tissues of two groups of mice (CON: n=6; IVF-ET: n=6); **b.** Expression levels of Rgs16 mRNA in liver tissues of mice in both groups (CON: n=6; IVF-ET: n=6); **c.** Protein expression of AKT, ERK1/2, p-ERK, p-AKT, GDF15, and RGS16 in liver tissues of both groups (CON: n=5-6; IVF-ET: n=5-6). For bar graphs, data represent mean+SEM. *, p<0.05; **, p<0.01. Relative to control, by two-tailed Student's t-test.

Figure 6

Relationship of GDF15 with lipid metabolism and RGS16. **a.** GDF15 and RGS16 mRNA expression levels after GDF15 knockout (si-NC: n=3; si-GDF15: n=3); **b.** Protein levels of AKT, ERK1/2, p-ERK1/2, p-AKT, GDF15 and RGS16 after GDF15 knockdown (si-NC: n=3-6; si-GDF15: n=3-6); **c.** mRNA expression levels of lipogenic and fatty acid oxidation genes after GDF15 knockdown (si-NC: n=3; si-GDF15: n=3); **d.** mRNA expression levels of GDF15, RGS16 after overexpression of GDF15 (pcDNA-empty: n=3; pcDNA-GDF15: n=3); **e.** Protein levels of AKT, ERK1/2, p-ERK1/2, p-AKT, GDF15 and RGS16 after overexpression of GDF15 (pcDNA-empty: n=3; pcDNA-GDF15: n=3); **f.** mRNA expression levels of lipogenic genes and fatty acid oxidation genes after overexpression of GDF15(pcDNA-empty: n=3-6; pcDNA-GDF15: n=3-6). HepG2: Human hepatocellular carcinoma cell line; si-GDF15: interfering RNA; si-NC: negative control for interfering RNA; pcDNA-GDF15: GDF15 overexpression plasmid; pcDNA-empty: empty plasmid (negative control). For bar graphs, data represent mean+SEM. *, p<0.05; **, p<0.01; ***, p<0.001; ****, p<0.001; ns, not significant. Relative to negative control, by two-tailed Student's t-test.

Figure 7

Effects of simultaneous knockdown of GDF15 and RGS16 on lipid metabolism. **a.** Oil Red O staining of HepG2 cells with si-NC, si-GDF15, si-RGS16 and si-GDF15+si-RGS16 (scale bar=50μm). **b.** Protein levels of ERK1/2, AKT, p-ERK1/2, p-AKT, GDF15 and RGS16 in si-NC, si-GDF15 and si-GDF15+si-RGS16 (si-NC: n=3; si-GDF15: n=3; si-GDF15+si-RGS16: n=3). **c.** mRNA expression levels of lipogenic and fatty acid oxidation genes of si-NC, si-GDF15 and si-GDF15+si-RGS16 (si-NC: n=3; si-GDF15: n=3; si-GDF15+si-RGS16: n=3). For bar graphs, data represent mean+SEM. si-NC vs si-GDF15: *, p<0.05; **, p<0.01; ****, p<0.001; ns, not significant. Relative to si-NC, by two-tailed Student's t-test. si-GDF15 vs si-GDF15+si-RGS16: #, p<0.05; ##, p<0.01; ####, p<0.001; ns, not significant. Relative to si-GDF15, by two-tailed Student's t-test.

Supplementary Files

This is a list of supplementary files associated with this preprint. Click to download.

- Additionalfile1TableS1toS4.docx
- Additionalfile2SupplementaryFigure1.docx
- Additionalfile3SupplementaryFigure2.docx
- additionalfile4.docx